

RESEARCH ARTICLE

The *Arabidopsis* stomatal polarity protein BASL mediates distinct processes before and after cell division to coordinate cell size and fate asymmetries

Yan Gong^{1,2}, Julien Alassimone^{1,*}, Andrew Muroyama^{1,†}, Gabriel Amador³, Rachel Varnau¹, Ao Liu² and Dominique C. Bergmann^{1,2,§}

ABSTRACT

In many land plants, asymmetric cell divisions (ACDs) create and pattern differentiated cell types on the leaf surface. In the *Arabidopsis* stomatal lineage, *BREAKING OF ASYMMETRY IN THE STOMATAL LINEAGE* (*BASL*) regulates division plane placement and cell fate enforcement. Polarized subcellular localization of *BASL* is initiated before ACD and persists for many hours after the division in one of the two daughters. Untangling the respective contributions of polarized *BASL* before and after division is essential to gain a better understanding of its roles in regulating stomatal lineage ACDs. Here, we combine quantitative imaging and lineage tracking with genetic tools that provide temporally restricted *BASL* expression. We find that pre-division *BASL* is required for division orientation, whereas *BASL* polarity post-division ensures proper cell fate commitment. These genetic manipulations allowed us to uncouple daughter-cell size asymmetry from polarity crescent inheritance, revealing independent effects of these two asymmetries on subsequent cell behavior. Finally, we show that there is coordination between the division frequencies of sister cells produced by ACDs, and this coupling requires *BASL* as an effector of peptide signaling.

KEY WORDS: Stomata, Asymmetric cell division, Cell polarity, Cell cycle, *BREAKING OF ASYMMETRY IN THE STOMATAL LINEAGE* (*BASL*), *EPIDERMAL PATTERNING FACTOR2* (*EPF2*)

INTRODUCTION

Cell polarity underlies many of the asymmetric and oriented cell divisions that create daughter cells with distinct fates (Drubin and Nelson, 1996; Muroyama and Bergmann, 2019). In both plants and animals, cell polarity frequently manifests as protein enrichment in specific subdomains of the cell, often associated with the plasma

membrane. During asymmetric cell division (ACD) in metazoans, spatially restricted ‘polarity proteins’ and their interaction partners orient cell division planes and recruit cell fate determinants to ensure asymmetric inheritance in daughter cells (Morin and Bellaïche, 2011). The general picture emerging from several decades of genetic analysis and protein-protein interaction studies is that polarity proteins act as scaffolds before division, both by recruiting clients that can guide spindle orientation and by creating environments that exclude proteins (e.g. cell fate determinants) from certain regions of the mother cell (Morin and Bellaïche, 2011).

Despite similar needs for cell polarity to orchestrate cellular and developmental behaviors, plants appear to employ a different suite of polarity proteins from those used in animals. One such protein, *BREAKING OF ASYMMETRY IN THE STOMATAL LINEAGE* (*BASL*), plays a central role in directing nuclear migrations to orient division planes, and in scaffolding intracellular signaling cascades to solidify differential cell fates in the *Arabidopsis* stomatal lineage (Dong et al., 2009; Muroyama et al., 2020; Zhang et al., 2016, 2015). The stomatal lineage features asymmetric, oriented and self-renewing divisions (Fig. 1A) and has emerged as a powerful model for investigating how cellular polarity specifies developmental patterns in plants.

A signature of stomatal lineage development, and a feature it shares with other plant developmental systems, is flexibility and tunability. The developmental trajectories of stomatal precursors are not fixed, and can be modulated by nutritional, hormonal and environmental cues (Engineer et al., 2014; Gong et al., 2021a; Han et al., 2020; Lau et al., 2018; Vatén et al., 2018; Wang et al., 2021). *BASL* polarity has been linked to this flexibility in several ways: *BASL* is employed to enforce cell fate commitment after ACDs (Dong et al., 2009; Muroyama et al., 2020; Zhang et al., 2016, 2015), and recent work has also correlated the persistence of *BASL* after ACD with self-renewing division capacity (Gong et al., 2021a). Roles of post-division polarity, particularly in regulating lineage flexibility, have been relatively understudied, in part because they are not features of the rapid and invariant cell divisions typical of invertebrate ACD models. In addition, there are structural differences between animal cells and walled plant cells, and these two branches of life use different cytoskeletal structures to dictate division planes and complete cytokinesis. Taken together, there remain numerous questions about the cellular and developmental mechanisms of ACDs in plants, for which a careful examination of *BASL* activities in the stomatal lineage might provide new or unexpected insights.


Here, we used time-lapse imaging, lineage tracing and quantitative polarity measurements to characterize how specific asymmetries in cell size, division rates, inherited factors, and orientation relative to landmarks affect cell fate and the overall pattern of the leaf epidermis. By creating genetic reagents to supply

¹Department of Biology, Stanford University, Stanford, CA 94305, USA. ²Howard Hughes Medical Institute, Stanford University, Stanford, CA 94305, USA.

³Department of Developmental Biology, Stanford University School of Medicine, Stanford, CA 94305, USA.

*Present address: Plant Pathology, Institute for Integrative Biology, ETH Zürich, CH 8092 Zürich, Switzerland. †Present address: Biological Sciences, UC San Diego, La Jolla, CA 92093, USA.

§Author for correspondence (dbergmann@stanford.edu)

 Y.G., 0000-0003-1329-7096; J.A., 0000-0002-8118-2605; A.M., 0000-0003-0701-212X; G.A., 0000-0002-6592-7136; R.V., 0000-0002-3203-9597; A.L., 0000-0003-0723-5315; D.C.B., 0000-0003-0873-3543

This is an Open Access article distributed under the terms of the Creative Commons Attribution License (<https://creativecommons.org/licenses/by/4.0>), which permits unrestricted use, distribution and reproduction in any medium provided that the original work is properly attributed.

Handling Editor: Yka Helariutta
Received 18 June 2021; Accepted 18 August 2021

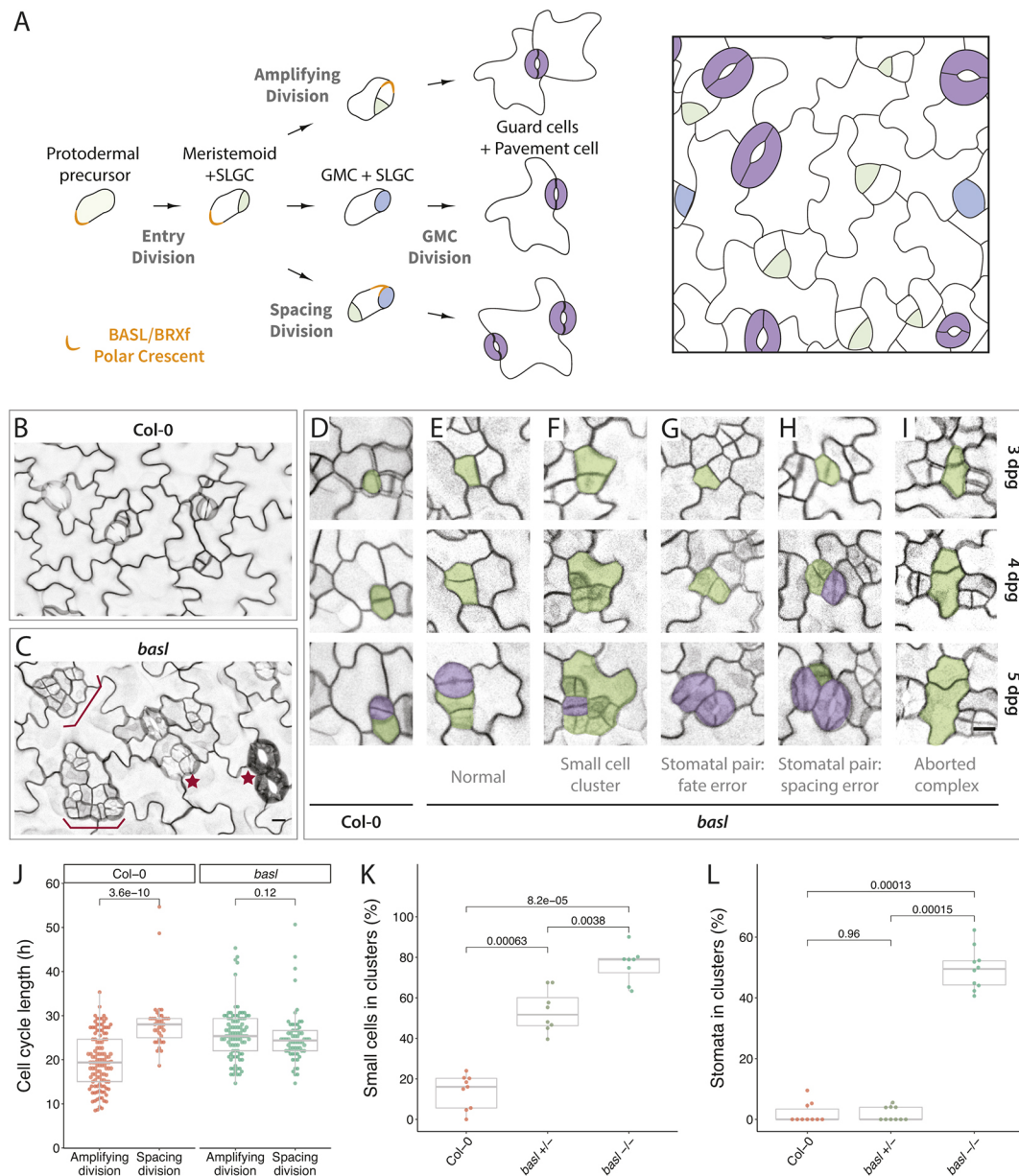


Fig. 1. Lineage tracing and quantitative analysis reveal multiple roles for BASL in the *Arabidopsis* stomatal lineage. (A) Schematic of stomatal lineage cell divisions with associated fate outcomes (left) and their arrangements on the leaf epidermis (right). Protodermal precursor cells enter the lineage and undergo asymmetric 'entry' divisions producing a smaller meristemoid (green) and a larger stomatal lineage ground cell (SLGC, white). Before division, BASL and partner proteins form a polar crescent at the cell cortex (orange); this crescent is inherited by the SLGC. Both meristemoids and SLGCs can undergo additional ACDs, termed amplifying divisions and spacing divisions, respectively. Alternatively, the SLGC can undergo terminal differentiation into a pavement cell and the meristemoid can transition into a guard mother cell (GMC, blue), undergo one symmetric division, and produce paired guard cells (purple). At any given time during leaf development, dispersed stomatal lineage cells are actively initiating, dividing and differentiating. (B,C) Confocal images of the abaxial epidermis of 5 dpv cotyledons from Col-0 (B) and *basl* (C) seedlings. Cell outlines are visualized by plasma membrane reporters *pATML1::RCI2A-mCherry* (Col-0) or *p35S::PIP2A-RFP* (*basl*). Brackets and stars indicate clustered small cells and stomata, respectively. (D-I) Examples of lineage-traced stomatal lineage cells from Col-0 (D) and *basl* (E-I) abaxial epidermis of cotyledons from 3 dpv to 5 dpv, showing the origins of normally patterned cell types (D,E), small cell clusters (F), stomatal pairs (G,H), and aborted complexes (I). Early stomatal lineage cells and stomata are false-colored in green and purple, respectively. (J) Cell cycle lengths among stomatal lineage cells from Col-0 ($n=147$ cells) and *basl* ($n=151$ cells) seedlings. Spacing and amplifying refer to divisions of the large and smaller daughter cell, respectively, that were created by the previous division. (K) Quantification of small cell clusters in the 5 dpv abaxial cotyledon epidermis ($n=8\ 388\times 388\ \mu\text{m}^2$ fields/genotype). The Bonferroni correction was applied to reduce Type I error, and the corrected P -value threshold for rejecting the null hypothesis (no difference between the mean of the compared groups) was calculated to be 0.017 (0.05/3). Any P -values below this corrected threshold were deemed significant. (L) Quantification of clustered stomata in 14 dpv abaxial cotyledon epidermis of the same genetic background as in K ($n=10\ 623\times 467\ \mu\text{m}^2$ fields/genotype, Bonferroni corrected P -value threshold=0.017). For all the box plots, the box represents the first and third quartiles with the middle line indicating median; the upper or lower whisker extends from the box to the largest or smallest value no further than 1.5 times the interquartile range. All P -values were calculated by Mann-Whitney test. Scale bars: 10 μm . See also Fig. S1.

BASL at discrete times over the course of asymmetric division, we show that BASL functions pre- and post-ACD are separable. Pre-division BASL is essential for division orientation whereas BASL

polarization post-division is necessary and sufficient for daughter cell fate asymmetry. Additionally, we discovered that supplying BASL post-division can uncouple cell size and polarity inheritance,

revealing a previously unappreciated role for BASL as an effector of sister-cell division coordination. Together, these results reveal how separable polarity modules can be coordinated by BASL to pattern ACDs in the leaf epidermis.

RESULTS

Loss of BASL abolishes fate asymmetry in ACD daughter cells and disrupts patterning of the leaf epidermis

To determine comprehensively the myriad functions of BASL during epidermal patterning, we re-examined the phenotypes of *BASL* null mutants (*basl-2*, hereafter referred to as *basl*) using time-lapse imaging and whole-leaf cell lineage tracing (Gong et al., 2021a). With this method, we tracked the developmental progression of all epidermal cells in the abaxial surface of wild-type Col-0 and *basl* cotyledons over 48 h (3–5 days post-germination, dpg). We observed that the *basl* abaxial epidermis exhibited an overall increase in cell number and numerous clusters of small cells and of mature stomata (Fig. 1B,C), in agreement with previous studies (Dong et al., 2009). Our lineage tracing revealed that small cell clusters typically form from excess divisions in both the larger and smaller cells born from an ACD (Fig. 1D–F). Clusters of mature stomata in the *basl* mutant arose from two independent origins.

First, as reported in the original characterization of *basl* (Dong et al., 2009), both daughter cells of a cell division could become guard mother cells (GMCs) and undergo symmetric cell divisions (GMC division) to form two adjacent stomata (Fig. 1G). Second, we found that stomatal pairs arose from misoriented spacing divisions, whereby a stomatal precursor cell is formed next to an existing stoma or GMC (Fig. 1H). Time-lapse imaging and lineage tracing over multiple days also revealed two previously unreported phenotypes in *basl*: (1) formation of ‘aborted complexes’ whereby both daughter cells of a seemingly asymmetric cell division acquired pavement cell fate (Fig. 1I), and (2) an equalization of cell cycle timing among daughter cells resulting from ACDs (Fig. 1J). Calculation of cell cycle length was especially interesting because, in contrast to many well-studied systems [e.g. the *Caenorhabditis elegans* embryo (Arata et al., 2014; Jankele et al., 2021) or the *Arabidopsis* shoot apical meristem (Jones et al., 2017)], the smaller daughter resulting from a stomatal lineage ACD has a shorter cell cycle time than the larger daughter.

This more precise and powerful phenotypic scoring system revealed an effect of *BASL* dosage on the small cell cluster phenotype (Fig. 1A,K), but not on the stomatal pair phenotype (Fig. 1L). This has interesting implications for the relationship between these two phenotypes, as it suggests that the excessive and incorrectly patterned small cells are not always destined to become incorrectly patterned stomata. Conversely, we found that stomatal clusters can arise from activities not linked to the production of small cell clusters (e.g. Fig. 1H). Because complete *BASL* loss of function profoundly alters cell identity and division patterns, and because of the non-linear relationship between early and terminal phenotypes, we reasoned that new genetic manipulation and analysis tools would be required to interrogate precisely *BASL* function during the cell cycle and throughout development.

Genetic reagents to supply BASL function pre- and post-division in asymmetrically dividing stomatal lineage cells

To dissect *BASL* function precisely, we designed three fluorescent *BASL* reporters to reintroduce *BASL* expression in a cell cycle-dependent manner during stomatal lineage ACDs (Fig. 2A). To restrict *BASL* expression to cells before division, we fused the *BASL*

coding sequence to the destruction box (DBox) motif of CYCLINB1;1, which targets the fusion protein for degradation during anaphase (Genschik et al., 1998), and placed this cassette under the native *BASL* promoter. We will refer to this pre-division *BASL* reporter (*pBASL::Venus-DBox-BASL*) as ‘*BASL*^{pre}’. To provide *BASL* primarily after division, we used the promoter of the cytokinesis-specific gene *KNOLLE* (Lauber et al., 1997) to drive fluorescently tagged *BASL* fused to a non-functional, mutated DBox (mDBox; Genschik et al., 1998). This post-division *BASL* reporter (*pKNOLLE::Venus-mDBox-BASL*) will be referred to as ‘*BASL*^{post}’. As a control, *BASL* was fused to the non-functional DBox and supplied in its complete expression range by *pBASL::Venus-mDBox-BASL*, referred to as ‘*BASL*^{full}’. Unless otherwise stated, all results reported below are from the expression of the indicated reporter in a *basl*^{-/-} mutant background. Fluorescence intensity of the Venus reporter was used to select lines expressing *BASL* protein variants at comparable levels (see Materials and Methods).

To test whether our temporally restricted *BASL* variants recapitulated typical polarity dynamics, we performed time-lapse imaging to monitor the expression patterns of *BASL*^{full}, *BASL*^{pre} and *BASL*^{post} during stomatal lineage ACDs (Fig. 2B,C). In these time-lapse studies, *BASL*^{full} polarity dynamics were similar to previously published functional translational reporters (Dong et al., 2009; Gong et al., 2021b). *BASL*^{full} was polarized at the cell cortex a few hours before cytokinesis (visualized by cell plate formation) and stayed polarized for more than 6 h after the division (Fig. 2B,C, top rows). *BASL*^{pre} was polarized only prior to cytokinesis, and *BASL*^{pre} signal was rapidly degraded (within one frame) after completion of cytokinesis (Fig. 2B,C, middle rows). In contrast, *BASL*^{post} was detected during cytokinesis (00:00) or one frame (40 mins) earlier (–00:40). *BASL*^{post} expression and polarity became more apparent several hours after division and persisted for a similar amount of time as *BASL*^{full} (Fig. 2B,C, bottom rows). Tracking *BASL* variants in individual cells revealed some variation in the duration of polarization (Fig. 2C), but, overall, the *BASL*^{pre} exhibited the same expression levels and behaviors of *BASL*^{full} (and previously published *BASL* reporters) before division, as did *BASL*^{post} after division. Notably, *BASL*^{post} could be highly polarized after division even when the reporter showed no polarity before division (Fig. 2C,D). *BASL* variants were also correctly oriented relative to landmarks, such as the nascent division plane, and each also accumulated in the nucleus (Fig. 2D).

To add more precision to the designation of ‘polarized’, we used the polarity quantification tool POME to measure the proportion of cell circumference occupied by the *BASL* reporters (Gong et al., 2021b). With POME, the distribution of cortically localized *BASL* in each cell was fitted to a Gaussian model and the standard deviation (s.d.) of this Gaussian model was extracted to represent the *BASL* crescent width quantitatively. To account for the fact that *BASL*^{pre} is expressed in meristemoids and *BASL*^{post} is expressed in stomatal lineage ground cells (SLGCs), we normalized polarity measurements as much as possible by analyzing cells of similar sizes. All three *BASL* variants could be highly polarized (Fig. 2E). Some less polarized cells were observed in *BASL*^{pre} and *BASL*^{full} reporter lines (outliers in Fig. 2E) and these likely correspond to meristemoids that have just initiated polarization, as has been documented before (Gong et al., 2021b).

BASL expression before division fails to rescue many aspects of asymmetric division

Having validated our temporally restricted *BASL* constructs, we tested whether *BASL*^{pre} and *BASL*^{post} could rescue the *basl* mutant

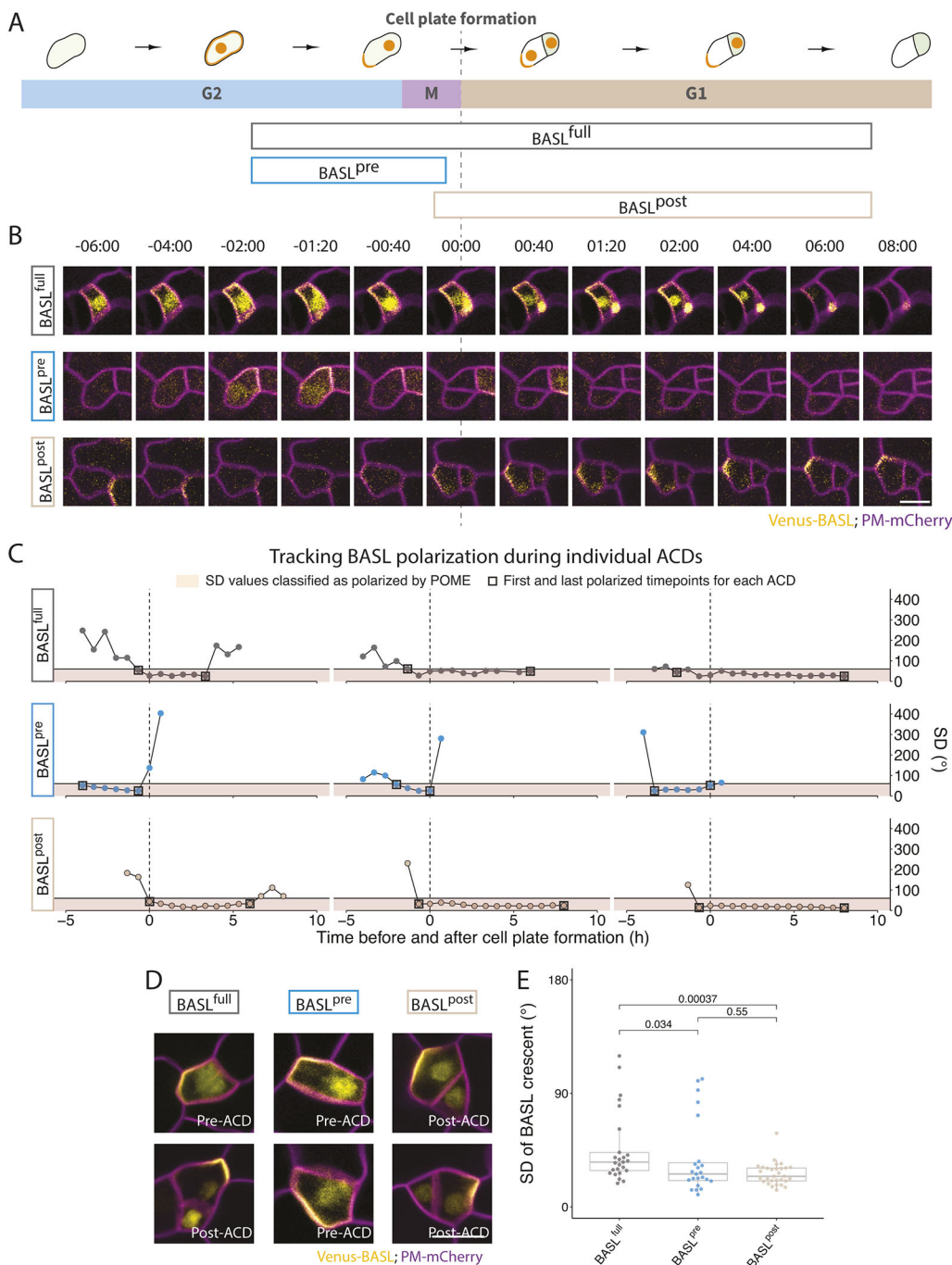


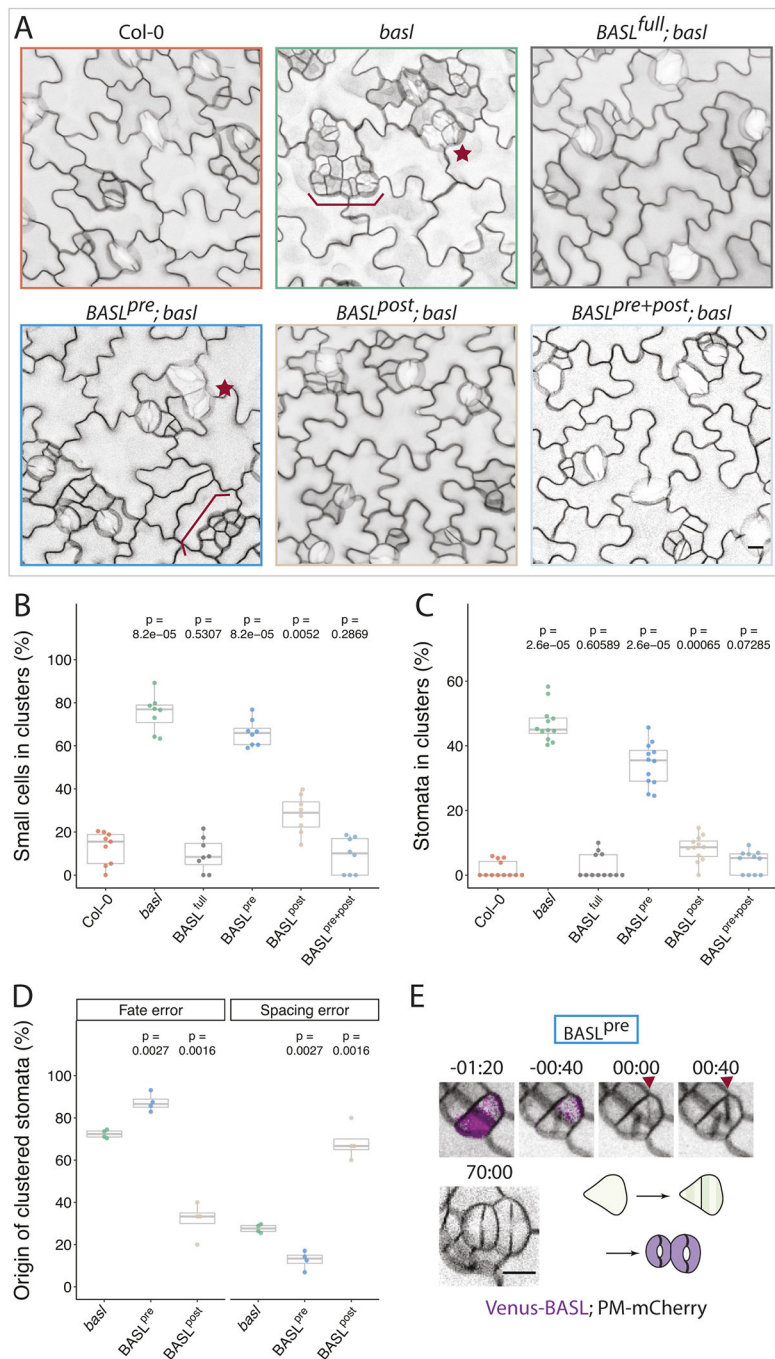
Fig. 2. Genetic reagents to control BASL expression timing during stomatal lineage divisions.

(A) Schematic illustrating the expression windows of $BASL^{full}$, $BASL^{pre}$ and $BASL^{post}$ variants during ACDs. (B) Time-lapse images showing localization dynamics of BASL variants (yellow) during a single cell division in 3 dpf cotyledons. 00:00 (h:min) marks cell plate formation. (C) Quantitative polarity tracking of BASL variants. For each polarized cell, the polarity crescent size is expressed as the standard deviation (s.d.) of the fitted Gaussian model of BASL cortical localization (see Materials and Methods). For each BASL variant, three individual cells were tracked using POME; each circle represents a time point and squares mark the first and last points below the s.d. value of 60° , used as the cut-off for polarization. Vertical dashed lines indicate the frames during which the cell plate forms, and all values in the pink zone are classified as polarized. (D,E) Comparison of crescent sizes among BASL variants, with two examples of each BASL variant (yellow) shown in D, and POME quantification of BASL crescent size (s.d.) of >20 cells/variant shown in E. In E, the Bonferroni corrected P -value threshold=0.017. In B and D, cell outlines (magenta) are visualized by the plasma membrane reporter $pATML1::RCI2A-mCherry$. For all the box plots, the box represents the first and third quartiles with the middle line indicating median; the upper or lower whisker extends from the box to the largest or smallest value no further than 1.5 times of the interquartile range. All P -values are calculated by Mann-Whitney test. Scale bars: 10 μ m.

phenotypes. First, we quantified the frequency of small cell clusters on the abaxial epidermis of developing (5 dpf) cotyledons (Fig. 3A,B) and the frequency of stomatal clusters, the terminal phenotype, on the abaxial epidermis of mature (14 dpf) cotyledons (Fig. 3C). $BASL^{full}$ completely rescued both phenotypes and resulted in a normally patterned epidermis (Fig. 3A), confirming that the addition of the mDBox motif did not interfere with the function of BASL. $BASL^{pre}$ largely failed to rescue, with cotyledons exhibiting numerous small cell and stomatal clusters. $BASL^{post}$, in contrast, mostly rescued stomatal clusters and partly rescued the small cell phenotype (Fig. 3A-C). Importantly, simultaneously introducing both $BASL^{pre}$ and $BASL^{post}$ into $basl$ fully rescued the mutant phenotypes (Fig. 3A-C), supporting the

idea that restricted temporal expression of BASL reveals discrete functions before and after division.

These results suggested that, not only was there a clear function for BASL after ACD, but that the post-divisional role might be more important than the pre-divisional role in defining stomatal lineage cell fates and patterning the leaf epidermis. Therefore, we performed a finer-grained phenotypic analysis to determine how $BASL^{pre}$ and $BASL^{post}$ affect cellular behavior. As shown in Fig. 1G,H, stomatal clusters in $basl$ had two origins: (1) a failure to establish differential fates in two sister cells and (2) misoriented spacing divisions. In $BASL^{pre}$, clustered stomata were mostly derived from fate errors, whereby both sisters divided symmetrically to create paired guard cells (Fig. 3D). In contrast, although the stomatal cluster phenotype



was substantially rescued by *BASL*^{post} (Fig. 3C), the residual clustered stomata in *BASL*^{post} arose from spacing errors, where SLGC spacing divisions were misoriented, creating new stomata next to existing ones (Fig. 3D, Fig. S1B). Thus, we observed a clear divergence in the origin of clusters when comparing *BASL*^{pre} and *BASL*^{post}. These results indicate that BASL contributes to different cellular and developmental processes before and after division, with pre-ACD BASL likely to regulate the orientation of ACDs, and post-ACD BASL enforcing cell fate differences in daughter cells. Indeed, extended time-lapse imaging and lineage tracing of lines lacking post-ACD BASL confirmed that cells undergoing morphologically normal ACDs can fail to separate fates correctly (Fig. 3E).

Presence of BASL before division coordinates crescent inheritance with daughter cell size asymmetry

In *BASL*^{post}, the BASL crescent sometimes appears in the smaller daughter cell (Fig. 4A, bottom right), a situation rarely seen in wild-type divisions. This gave us the unique opportunity to test whether BASL directly regulated cell size asymmetry, whether it coordinated size asymmetry with crescent inheritance, and ultimately whether cell size or crescent inheritance was the dominant factor in subsequent cell behavior. By quantifying the ratio of the surface area of the meristemoid to that of the SLGC in the frame following division (Fig. 4B), we found that meristemoids were typically half the area of SLGCs in wild-type

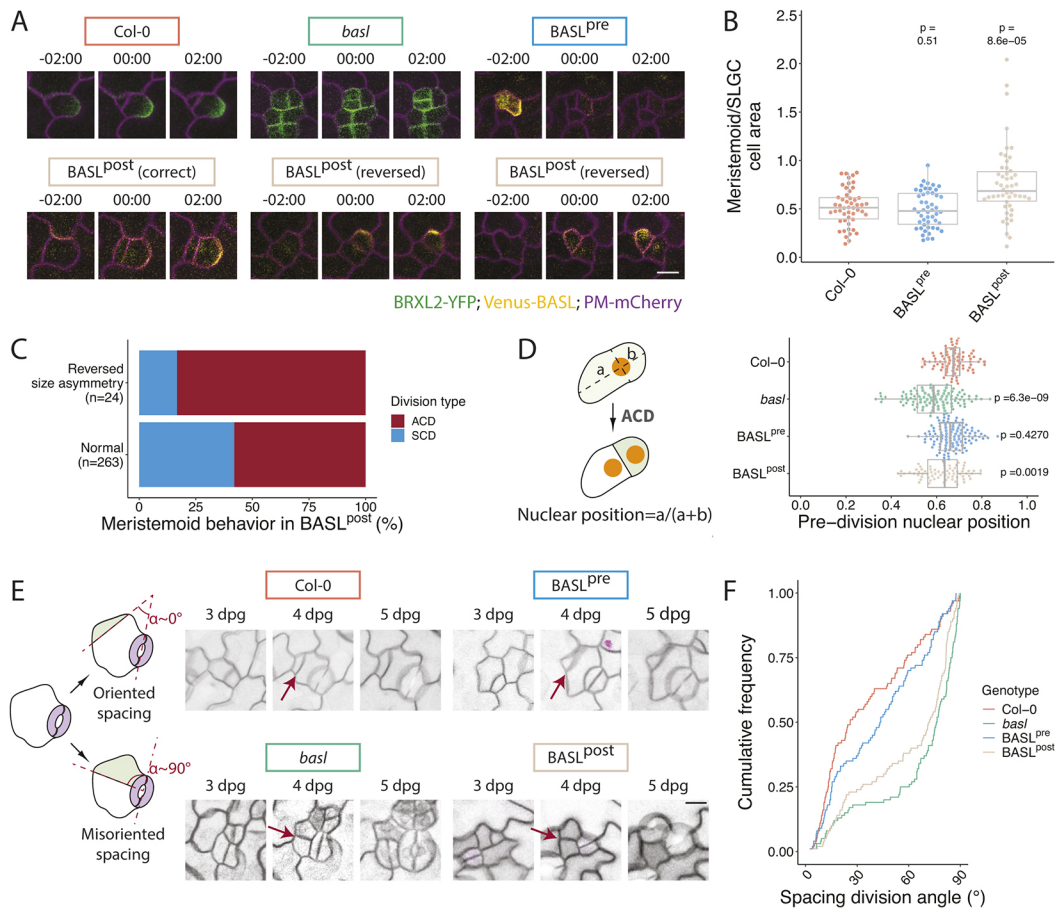


Fig. 4. Presence of BASL before division influences division plane placement and coordinates crescent inheritance with cell size asymmetry. (A) Time-lapse images of ACDs in 3 dp cotyledons of Col-0, *basl* and BASL variants. Cell outlines are visualized by the plasma membrane reporter (magenta) *pATML1::RCI2A-mCherry* or *p35S::PIP2A-RFP*. 00:00 (h:min) marks cell plate formation. Polarity domains are labeled with *pBRXL2::BRXL2-YFP* (green, in Col-0 and *basl*) or by BASL variants (yellow). Examples of *BASL^{post}* include two divisions in which the smaller daughter cell inherits the BASL crescent (reversed). (B) Quantification of cell size asymmetries from the genotypes in A, excluding *basl* because relationships between daughter cell size and crescent inheritance cannot be assigned ($n=50$ cells/genotype). (C) Quantification of meristemoid behaviors in *BASL^{post}* following divisions that exhibit normal and reversed size asymmetries. (D) Quantification of the final nuclear position pre-division in the indicated genotypes ($n>70$ cells/genotype, Bonferroni corrected P -value threshold=0.017). Schematic shows how pre-division nuclear position is defined. (E) Examples of spacing division orientations; α represents the angle between the stomatal pore axis and the axis of the new division plane. Red arrows point to examples of scored divisions. (F) Graph of the cumulative frequencies of spacing division angles (from 0° to 90°) for each genotype in E ($n=100$ cells/genotype). For all the box plots, the box represents the first and third quartiles with the middle line indicating median; the upper or lower whisker extends from the box to the largest or smallest value no further than 1.5 times of the interquartile range. All P -values are calculated by Mann-Whitney test and all pairwise P -values comparing individual genotypes to Col-0 are presented. Scale bars: 10 μ m.

and in *BASL^{pre}*. In *BASL^{post}* plants, however, meristemoid and SLGC sizes were more equalized, and we repeatedly identified cell pairs with ‘reversed’ polarity, where the BASL crescent polarized in the smaller cell. Lineage tracing revealed that BASL presence was a better predictor of subsequent behavior than cell size, as the daughter cell with the BASL crescent, regardless of its size relative to its sister, always acquired the SLGC fate. Interestingly, the reversed cell size asymmetry also had consequences for the cell lacking the BASL crescent. These large ‘meristemoids’ underwent subsequent amplifying divisions more frequently than meristemoids produced from divisions with normal meristemoid/SLGC size asymmetry (Fig. 4C). Thus, polarized BASL has a dominant impact on cell fate establishment, whereas cell size appears to influence the long-term self-renewing capacity of stomatal lineage stem cells.

BASL expression before division directs nuclear migration to create cell size asymmetries and to orient spacing divisions

Of the events comprising an ACD, we expected division plane placement to require pre-division polarity. Recent work has linked

division plane position to BASL-directed nuclear migrations in the stomatal lineage (Muroyama et al., 2020). To test whether the reduced cell size asymmetry could be due to nuclear migration defects, we introduced a nuclear marker (*pATML1::H2B-YFP*) into the BASL variant lines and characterized nuclear movements with time-lapse analysis. Pre-ACD nuclear migration was impaired in *BASL^{post}* and *basl*, as evidenced by the more centered position of the nucleus just prior to cell division (Fig. 4D). This failure in nuclear migration provides an explanation for how cell size can be uncoupled from the presence of a polar crescent in *BASL^{post}* plants.

Orienting division planes to avoid the creation of stomata in contact may be an even more crucial role for pre-ACD BASL than regulating cell size asymmetry in the stomatal lineage. During spacing divisions, the division plane is placed away from the existing stoma or stomatal precursor to avoid the formation of stomata pairs (Fig. 4E, left), and this oriented division pattern is dependent on BASL activity (Figs 1H, 3D). We reasoned that the ability of BASL to orient spacing divisions relies mostly on its ability to direct pre-divisional nuclear migration. This hypothesis was supported by lineage-tracing

experiments in which we observed more misoriented spacing divisions in the cotyledons of *basl* and *BASL^{post}* plants (Fig. 4E). Quantification of spacing division angle in these genetic backgrounds revealed that without pre-ACD *BASL* activity, the ability of the SLGC to orient spacing division was compromised, and more spacing divisions were positioned orthogonally to existing stomata (Fig. 4F). Many cases of such misoriented spacing divisions led to the formation of stomatal pairs (Fig. 4E, right). Taken together, the behavior of *BASL^{pre}* and *BASL^{post}* suggest that *BASL* fulfills discrete and separable roles in mother and daughter cells of an ACD.

Presence of *BASL* after division coordinates division propensity between sister cells resulting from ACDs

A prominent phenotype in *BASL^{pre}*, in addition to the stomatal clusters arising from cell fate defects, was an excessive number of clustered small cells (Fig. 3B). The arrangement of cells in these clusters suggested that both daughters of an ACD divided more frequently than in wild type (Fig. 5A). This phenotype was also prominent in *basl* but not in *BASL^{post}* (Fig. 5A). In lineage traces of cells in the wild-type Col-0 cotyledon epidermis (followed from 3-5 dpq), we noticed that spacing divisions were less frequent in

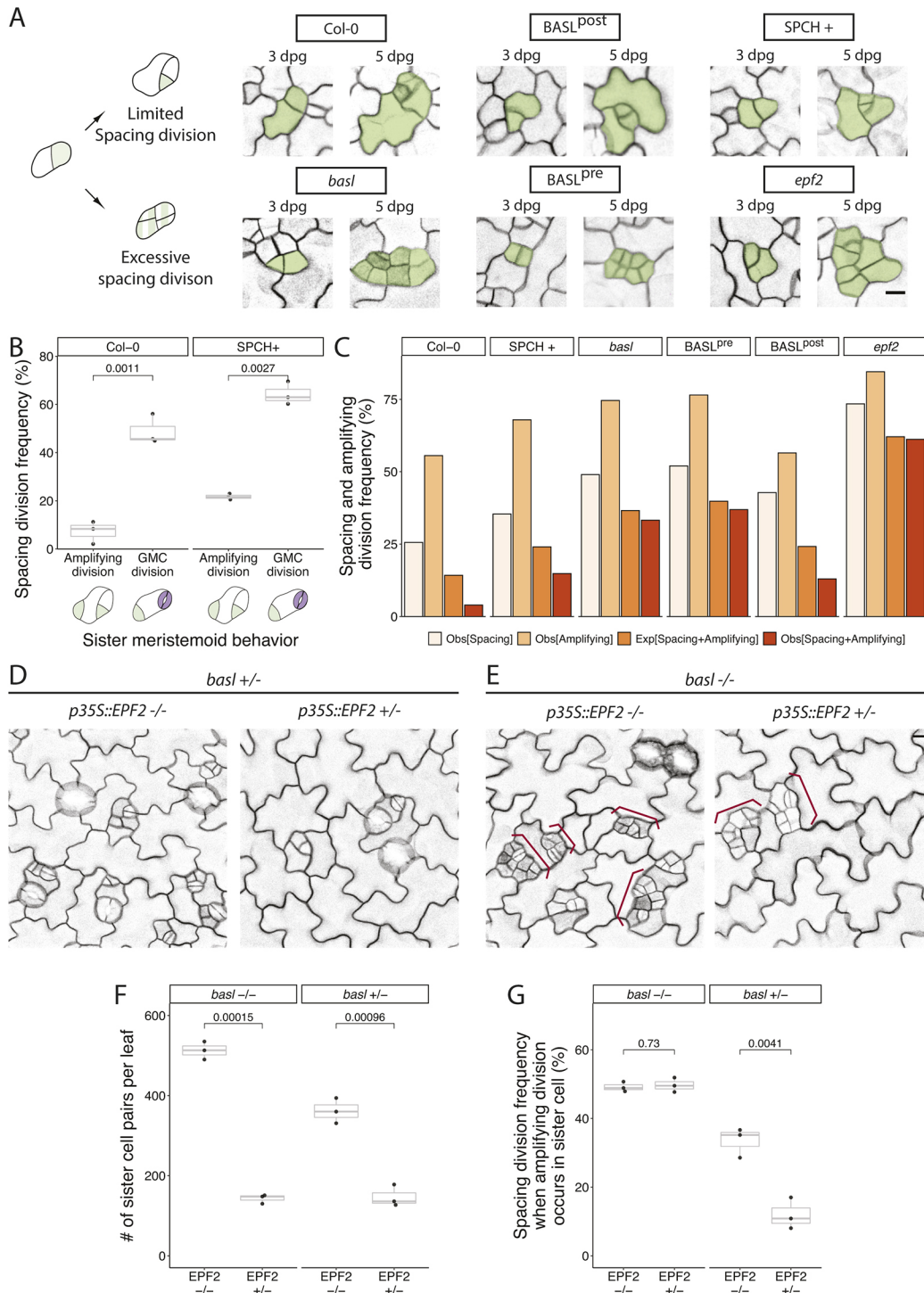


Fig. 5. See next page for legend.

Fig. 5. Presence of BASL post-ACD ensures cell fate asymmetry and coordinates sister cell divisions. (A) Schematic and examples of how excessive spacing divisions form small cell clusters. Top row gives examples of normal lineages in which meristemoid amplifying divisions are associated with limited SLGC spacing divisions. Bottom row shows examples of both amplifying and spacing divisions occurring in neighboring sisters. Tracked stomatal lineage cells are false-colored in green. (B) Division frequencies are coordinated between sister cells when overall divisions are elevated through increased SPCH dosage (SPCH+). Frequencies are calculated by tracing the subsequent division behaviors of the daughters of an asymmetric division ($n=3$ cotyledons/genotype; $n>300$ pairs/cotyledons tracked from 3-5 dp). (C) Quantification of observed spacing division frequency (Obs[SPA]), observed amplifying division frequency (Obs[AMP]), observed frequency of both amplifying division and spacing division (Obs[SPA+AMP]), and the expected frequency of amplifying division and spacing division (Exp[SPA+AMP]) under the assumption that these two divisions were independent (calculated by multiplying Obs[AMP] by Obs[SPA]; $n>500$ pairs/genotype). (D) Suppression of entry and spacing divisions by overexpression of EPF2 ($p35S::EPF2$) in $BASL^{+/-}$ plants. (E) Suppression of entry divisions, but not spacing divisions, by $p35S::EPF2$ in $basl^{-/-}$. (F,G) Quantification of entry divisions (F; estimated by the number of actively dividing pairs of sister cells at 3 dp) and sister cell division coordination (G; estimated by the spacing division frequency when amplifying division occurs in sister meristemoid) from the genotypes shown in D,E. Both results in F,G are quantified from whole-leaf lineage-tracing experiments ($n=3$ cotyledons/genotype tracked from 3-5 dp; $n>120$ pairs/cotyledons in $p35S::EPF2$ lines; $n>300$ pairs/cotyledons in lines not expressing $p35S::EPF2$). In D,E, cell outlines are visualized by the plasma membrane reporter $pATML1::RCI2A-mCherry$ and small cell clusters are labeled with red braces. For all the box plots, the box represents the first and third quartiles with the middle line indicating median; the upper or lower whisker extends from the box to the largest or smallest value no further than 1.5 times of the interquartile range. All P -values are calculated by Student's t -test due to small sample size. Scale bars: 10 μ m.

SLGCs for which the sister meristemoid underwent an amplifying division and more frequent in SLGCs for which the sister meristemoid differentiated into a GMC (and ultimately became guard cells) (Fig. 5B). This suggested some type of coordination between the division propensity of sister cells. We quantified the extent of potential coordination by tracking how often both a spacing division and an amplifying division occurred in a pair of sister cells (Obs[SPA+AMP]) and comparing this with the expected frequency if spacing and amplifying divisions were independent events (Exp[SPA+AMP]; see details in Materials and Methods). We found a large difference between expected and observed frequencies in wild-type Col-0 (Fig. 5C). To test whether this presumed coordination between sisters was robust to increases in overall division frequency, we quantified divisions in plants expressing an additional copy of the transcription factor SPEECHLESS ($pSPCH::SPCH-CFP$ or SPCH+) (Davies and Bergmann, 2014). Although both types of ACDs were elevated in SPCH+ (Fig. 5B), SLGC spacing division propensity was still highly correlated with the division behavior of its sister (Fig. 5B,C). Interestingly, the coordination between sister cell divisions was diminished in $basl$ and $BASL^{pre}$ plants but maintained in $BASL^{post}$ plants (Fig. 5C). This suggests that meristemoid/SLGC sister cell pairs communicate to coordinate spacing and amplifying divisions via BASL activity post-ACD, and that excessive divisions and small cell clusters result from a failure in communication.

How might BASL help coordinate cell division frequency between stomatal lineage sister cells? One hypothesis is that the peptide ligand EPIDERMAL PATTERNING FACTOR2 (EPF2), produced by meristemoids, signals to its sister SLGC. EPF2 was previously shown to suppress ACDs in neighbor cells through activating MITOGEN ACTIVATED PROTEIN KINASE (MAPK) signaling (Han and Torii, 2016; Hara et al., 2009; Hunt and Gray,

2009). MAPK signaling, in turn, is facilitated by BASL-mediated scaffolding post-ACD (Zhang et al., 2015). We re-examined the $epf2$ loss-of-function mutant and found that, like $basl$ and $BASL^{pre}$, the phenotype included excessive spacing divisions and a lack of sister cell division coordination (Fig. 5A,C). We then asked whether BASL was required for this EPF2-dependent inhibition of spacing divisions. Overexpression of EPF2 has a dose-dependent effect on ACDs (Lee et al., 2015) and by expressing a $p35S::EPF2$ construct, we were able to generate lines in which most, but not all, divisions were reduced. By crossing one such $p35S::EPF2$ line made in a $basl$ background to $basl$ or Col-0 plants and assaying phenotypes in the F1 generation, we tested whether $BASL$ mediated the reduction in divisions. Overexpression of EPF2 suppressed both stomatal entry divisions and spacing divisions in $BASL^{+/-}$ (Fig. 5D,F,G), whereas overexpression of EPF2 in $basl^{-/-}$ suppressed only entry divisions but not the excessive spacing divisions (Fig. 5E-G). $BASL$ is therefore required for EPF2-driven division suppression, and EPF2 appears to be the signal coordinating the trade-off between division propensity of meristemoids and their sister SLGCs.

DISCUSSION

Polarity domains can act as hubs to coordinate multiple cellular behaviors across the cell cycle. Our understanding of how these potentially independent functions are coordinated in plant cells, however, has been limited by the resolution of traditional mutant phenotype analysis. Here, we developed new experimental approaches for quantitative analysis of developmental dynamics of the *Arabidopsis* stomatal lineage, enabling new insights into the rules that govern cell behaviors and tissue patterning. Our temporal dissection of BASL function confirmed previous models implicating $BASL$ in the regulation of nuclear migration before division and reinforcement of cell fate after division (Dong et al., 2009; Muroyama et al., 2020; Zhang et al., 2016). In addition, our data extend previous models of BASL function in two significant ways. First, our $BASL^{post}$ data suggest that polarized BASL does not need to be inherited through the division but can function when formed *de novo* after ACD. Second, our system allowed us to uncouple cell size and polarity status, which are typically highly correlated in stomatal lineage divisions. The post-division activities of BASL are particularly interesting because most of the current literature on polarity proteins during ACDs focuses on their roles in regulating cellular processes such as spindle orientation and fate determinant segregation before division. The *Arabidopsis* stomatal lineage, with its long cell cycles and incorporation of cell growth between divisions, contrasts with well-studied ACD models such as *C. elegans* embryos or *Drosophila* neuroblasts, but is representative of the typical situation in plant and mammalian development (Francis et al., 2008; Gonsalvez et al., 2015; Jedrusik et al., 2010).

Building from the observation that, during the long cell divisions of the *Arabidopsis* stomatal lineage, polar cortical domains persist for hours after division (Gong et al., 2021a,b), we had an opportunity to use genetic tools to supply BASL before and after division to dissect its roles at those stages. We concluded that the ability of BASL to generate fate asymmetry in ACD daughter cells largely depends on its post-divisional polarity, a different result from classical ACD systems; for example, in *Drosophila* neuroblasts the differential inheritance of fate determinant factors such as Numb, Prospero and Brat, depends on PAR polarity prior to ACD (Homem and Knoblich, 2012). We propose two hypotheses for why the stomatal lineage appears to emphasize post-divisional activities: (1) in a flexible system, it may be that segregated determinants bias a cell fate decision but can be overridden by

signaling or other events post division or (2) polarized BASL and the signaling molecules it scaffolds are themselves the fate-determining factors. In either case, post-ACD BASL is required to maintain the separate cell fates.

Another interesting comparison between animal models and the stomatal lineage is the effect of cell size on asymmetric divisions. Divisions creating daughters of unequal sizes are common during development, but whether cell size per se matters for fate is not clear. Recent work experimentally equalizing cell size in *C. elegans* embryos showed effects on cell cycle timing and on developmental progression (Jankele et al., 2021). In our work, we found that cell size did not correlate with cell divisions in the same way; rather than larger cells dividing faster as in *C. elegans*, small cells of the stomatal lineage divided faster, though loss of polarity proteins equalized timings in both situations. In terms of fate, smaller daughters of an ACD that expressed BASL^{post} (in the case of ACD size asymmetry reversal) still became pavement cells, suggesting that size was not crucial for cell identity during stomatal lineage ACDs. Cell size, however, did affect the number of divisions the non-BASL inheriting cell underwent (Fig. 4C), suggesting that in this flexible stem cell-like lineage, cell size asymmetry may be important for regulation of overall division capacity.

Investigation of the small cell cluster phenotype was particularly fruitful for refining and defining new roles for BASL. First, we found that *BASL* was haploinsufficient for this phenotype, suggesting that the mechanisms regulating cell division propensity are more sensitive to BASL dosage than those that are required for cell fate. Because the stomatal clustering phenotype is completely recessive, it indicates that the small cell clusters can be resolved without affecting overall stomata patterning, which suggests additional layers of regulation that enable error correction. Second, lineage tracing of cells in small cell clusters revealed a previously unappreciated coordination between the division behaviors of meristemoids and their sister SLGCs. Our data indicate that BASL is an effector of EPF2-mediated signaling between sister cells that prevents both cells from undergoing ACDs. This finding forces us to consider the idea that polarity domains can have non-cell-autonomous effects; future studies might determine whether this mechanism occurs in other contexts and whether the non-autonomous effects are chemical (signaling) or mechanical in nature. Why might stomatal lineage sister cells coordinate their divisions? Coordination could serve as a patterning mechanism to prevent divisions that would place guard cell precursors in contact. Alternatively, plants alter stomatal indices (SI, the ratio of stomatal to non-stomatal epidermal cells) in response to systemic and environmental cues. However, amplifying and spacing divisions have opposite effects on SI, with amplifying divisions decreasing, and spacing divisions increasing SI. The antagonistic behaviors of sisters may reflect circuitry designed to amplify cues that instruct the tissue to modulate SI in response to environmental stimuli.

MATERIALS AND METHODS

Plant material and growth conditions

All *Arabidopsis* lines used in this study are in the Col-0 background. All *Arabidopsis* seeds were surface-sterilized by bleach or 75% ethanol and stratified for 2 days. After stratification, seedlings were vertically grown on ½ Murashige and Skoog (MS) media with 1% agar for 3-14 days under long-day conditions (16 h light/8 h dark at 22°C) and moderate intensity full-spectrum light (110 µE).

Previously reported mutants and transgenic lines include: *epf2* (Hunt and Gray, 2009), *pATML1::RCI2A-mCherry* (Bringmann and Bergmann, 2017), *p35S::PIP2A-RFP* in *basl-2* (Rowe et al., 2019 preprint), *pATML1::H2B-YFP* *p35S::PIP2A-RFP* in *basl-2* (Muroyama et al.,

2020), *pATML1::mCherry-RCI2A* *pRPS5A::DII-n3xVenus* *pRPS5A::mDII-ntdTomato* *pBRXL2::BRXL2-YFP* (Muroyama et al., 2020), and *pSPCH::SPCH-YFP* (Davis and Bergmann, 2014).

Newly generated lines include: *pBASL::Venus-mDBox-BASL* *pATML1::mCherry-RCI2A* in *basl-2*, *pBASL::Venus-DBox-BASL* *pATML1::mCherry-RCI2A* in *basl-2*, *pKNOLLE::Venus-mDBox-BASL* *pATML1::mCherry-RCI2A* in *basl-2* and *p35S::EPF2* *p35S::PIP2A-RFP* in *basl-2*. For nuclear migration assays, the BASL variants were crossed with *pATML1::H2B-YFP* *p35S::PIP2A-RFP* in *basl-2*, and plants were scored in F1s as the large number of transgenes lead to silencing in later generations. To ensure the same dose of EPF2 overexpression, *p35S::EPF2/+* *p35S::PIP2A-RFP* in *basl-2* was crossed to either *pATML1::RCI2A-mCherry* (Col-0) or *p35S::PIP2A-RFP* in *basl-2* and phenotypic assays were performed in F1 seedlings. For BASL^{full} (*pBASL::Venus-mDBox-* in *basl-2*), BASL^{pre} (*pBASL::Venus-DBox-BASL* in *basl-2*) and BASL^{post} (*pKNOLLE::Venus-mDBox-BASL* in *basl-2*), T2 lines were evaluated for reporter fluorescence intensity. After confirming that BASL^{full} completely rescued *basl* ACD phenotypes, lines bearing BASL^{pre} and BASL^{post} variants with fluorescence intensity similar to BASL^{full} before and after division, respectively, were used for all subsequent functional analysis.

Vector construction and plant transformation

To generate *pBASL::Venus-DBox-BASL*, the coding sequence of the destruction box (DBox) domain of *Arabidopsis* CYCB1;1 (first 116 amino acids) (Genschik et al., 1998) was fused with the coding sequence of fluorescent protein Venus utilizing a BamHI restriction site, cloned into Gateway vector pENTR (Thermo Fisher), and recombined with entry vectors containing the *BASL* promoter (3 kb) and the *BASL* coding sequence into binary vector pK7m34GW (Karimi et al., 2007). Similar approaches were used to generate *pBASL::Venus-mDBox-BASL* and *pKNOLLE::Venus-mDBox-BASL* with the *BASL* and 2.4 kb *KNOLLE* promoters, respectively. mDBox contains the same region of *Arabidopsis* CYCB1;1 as DBox, but with the motif RxxLxx(L/I)xN changed to GxxVxx(L/I)xN (Genschik et al., 1998). To generate *p35S::EPF2*, the *EPF2* coding sequence was cloned into pENTR and recombined into the pH35GS binary vector (Kubo et al., 2005). Transgenic plants were then generated by *Agrobacterium*-mediated transformation (Clough and Bent, 1998), and transgenic seedlings were selected on ½ MS plates with 50 µg/ml hygromycin (pH35GS; Thermo Fisher) or 50 µg/ml kanamycin (pK7m34GW; Sigma) antibiotics. Primers used to create these constructs are listed in Table S1.

Microscopy, image acquisition and image analysis

All fluorescence imaging experiments were performed on a Leica SP5 confocal microscope with HyD detectors using 40× NA1.1 water objective with image size 1024×1024 and digital zoom from 1× to 2×.

For time-lapse experiments, 3 dpg seedlings were mounted in a custom imaging chamber (Davies and Bergmann, 2014) filled with ½ MS solution. For the time-lapse experiments reported in this study, there was a 30-45 min interval between each image stack capture. For the time-lapse followed by time-course experiments, seedlings were imaged in the time-lapse chamber for 16 h as above. After imaging, seedlings were removed from the imaging chamber and returned to MS-agar plates (with appropriate supplements) for 48 h under standard light and temperatures. The same epidermal surface from the same plant was re-imaged to capture the developmental outcome of all the epidermal cells. Whole leaf-based time-course and lineage-tracing experiments were performed as described by Gong et al. (2021b). Quantification of nuclear migration was carried out as described by Muroyama et al. (2020).

Quantification of BASL polar crescent size was performed with the Fiji plugin POME (Gong et al., 2021b). Twenty to thirty highly expressing cells were selected, and the BASL localization pattern in each of these cells was analyzed by POME and fitted to a Gaussian model to extract key parameters of BASL localization pattern. These parameters included standard deviation σ , center μ , amplitude α and baseline value β . The standard deviation (σ) from the regression model of each cell's BASL localization pattern was then defined as the crescent size. The crescent sizes of all analyzed cells from BASL variants were then plotted and compared.

To quantify the small cell cluster phenotype, seedlings bearing a fluorescent cell outline marker were imaged at 5 dpw with a $388 \times 388 \mu\text{m}^2$ field of view. Each individual image was segmented in Fiji. Cells with surface area smaller than $120 \mu\text{m}^2$ were considered small cells. To simplify the analysis, we used cell area instead of cell volume as epidermal cell height (distance from apical to internal face) is quite uniform at the cotyledon ages we measured (Muroyama et al., 2020). Four or more small cells in contact were considered a cluster and the fraction of small cells in clusters/total small cells was counted. To count clusters of mature stomata, seedlings were collected at 14 dpw. Samples were cleared with 7:1 solution of ethanol:acetic acid, treated with 1 N potassium hydroxide solution, rinsed in water, and then mounted in Hoyer's solution. Individual leaves were then imaged with a Leica DM6B microscope with a $20 \times$ NA0.7 air objective in differential interference contrast (DIC) mode. Total stomata number and the number of stomata in direct contact were counted to calculate the percentage of stomata in clusters. The origin of a given stomatal cluster was determined from lineage tracing of whole-leaf time courses (3 dpw to 5 dpw). Stomatal clusters generated from a pair of sister cells from a cell division were classified as fate errors whereas any stomatal clusters generated from a misplaced spacing division were classified as spacing errors.

To determine whether sister cell division propensities were correlated, we tracked sister cell pairs for 48 h (3-5 dpw). We then calculated the frequencies of spacing and/or amplifying divisions among tracked cells. The observed spacing division frequency $\text{Obs}[\text{SPA}]$ is the number of SLGCs in which a spacing division occurred divided by the total number of tracked SLGCs. The observed amplifying division frequency $\text{Obs}[\text{AMP}]$ is the number of meristemoids in which an amplifying division occurred divided by the total number of tracked meristemoids. $\text{Obs}[\text{SPA}+\text{AMP}]$ is the observed frequency of meristemoids undergoing an amplifying division and their sister SLGC undergoing a spacing division divided by the total number of tracked sister pairs. From the lineage-tracing data, we also computed $\text{Exp}[\text{SPA}+\text{AMP}]$, the expected frequency of a pair of sister cells undergoing an amplifying division and a spacing division if these two divisions were independent of each other, by multiplying $\text{Obs}[\text{SPA}]$ and $\text{Obs}[\text{AMP}]$. Deviations of $\text{Obs}[\text{SPA}+\text{AMP}]$ from $\text{Exp}[\text{SPA}+\text{AMP}]$ suggest interactions between sisters, with a lower $\text{Obs}[\text{SPA}+\text{AMP}]$ relative to $\text{Exp}[\text{SPA}+\text{AMP}]$ indicative of competition or inhibition between sisters. The division behaviors of at least 500 cell pairs were tracked for each genotype.

Statistical analysis

All statistical analyses in this study were performed in RStudio. Unpaired Mann–Whitney tests and Student's *t*-tests were conducted to compare two data samples with the `compare_means` function from the `ggpubr` package (<https://CRAN.R-project.org/package=ggpubr>). For all graphs, sample sizes of each group and *P*-values from the unpaired Mann–Whitney tests or Student's *t*-test are directly labeled on these graphs or stated in the figure legends. Bonferroni corrections were performed when more than two pairwise comparisons were conducted to reduce Type I error. Bonferroni corrected *P*-value thresholds are indicated in the corresponding figure legends. When counting stomata and small cell clusters, labels revealing the identity (genotype) of samples were temporarily removed from confocal and DIC image files to minimize scoring bias. For quantification of stomata clusters using DIC images of 14 dpw *Arabidopsis* seedlings mounted in Hoyer's solution, only images with clear cell boundaries were included. For the lineage-tracing experiments, only seedlings of similar size and developmental stages (judged by root length and cotyledon size) were selected for analysis. For all the boxplots in the figures, all data points are shown as individual dots accompanying summarized boxes. For each box, the upper and lower hinges of each box represent the third and first quartiles; the upper whisker extends from the upper hinge to the largest value no further than 1.5 times of the interquartile range; the lower whisker extends from the lower hinge to the smallest value no further than 1.5 times of interquartile range.

Acknowledgements

We thank the members of the Bergmann lab for discussions and feedback on the manuscript and Chin-Min Kimmy Ho (now at IPMB, Academia Sinica, Taiwan) for constructs.

Competing interests

The authors declare no competing or financial interests.

Author contributions

Conceptualization: Y.G., J.A., D.C.B.; Methodology: Y.G., J.A., A.M.; Validation: Y.G., J.A., A.M., G.A., R.V.; Formal analysis: Y.G., A.M.; Investigation: Y.G., J.A., A.M., G.A., R.V., A.L.; Writing - original draft: Y.G., J.A., A.M., G.A., D.C.B.; Writing - review and editing: Y.G., D.C.B.; Visualization: Y.G., A.M.; Supervision: D.C.B.; Project administration: D.C.B.; Funding acquisition: J.A., A.M., G.A., D.C.B.

Funding

J.A. was supported by postdoctoral fellowships Schweizerischer Nationalfonds zur Förderung der Wissenschaftlichen Forschung (EPM – PBLAP3-142757 and APM – P300P3-158432) and from the European Molecular Biology Organization (ALTF – 878-2013). A.M. was supported by a postdoctoral fellowship from the National Institutes of Health (F32 GM133102). G.A. is supported by funds from the National Institutes of Health (T32 5T32GM007790), the National Science Foundation (DGE-1656518) and a Stanford Graduate Fellowship. D.C.B. is an investigator of the Howard Hughes Medical Institute. Open access funding provided by Stanford University. Deposited in PMC for immediate release.

Peer review history

The peer review history is available online at <https://journals.biologists.com/dev/article-lookup/doi/10.1242/dev.199919>

References

- Arata, Y., Takagi, H., Sako, Y. and Sawa, H. (2014). Power law relationship between cell cycle duration and cell volume in the early embryonic development of *Caenorhabditis elegans*. *Front. Physiol.* **5**, 529. doi:10.3389/fphys.2014.00529
- Bringmann, M. and Bergmann, D. C. (2017). Tissue-wide mechanical forces influence the polarity of stomatal stem cells in *Arabidopsis*. *Curr. Biol.* **27**, 877-883. doi:10.1016/j.cub.2017.01.059
- Clough, S. J. and Bent, A. F. (1998). Floral dip: a simplified method for *Agrobacterium*-mediated transformation of *Arabidopsis thaliana*. *Plant J.* **16**, 735-743. doi:10.1046/j.1365-3113x.1998.00343.x
- Davies, K. A. and Bergmann, D. C. (2014). Functional specialization of stomatal bHLHs through modification of DNA-binding and phosphoregulation potential. *Proc. Natl. Acad. Sci. USA* **111**, 15585-15590. doi:10.1073/pnas.1411766111
- Dong, J., MacAlister, C. A. and Bergmann, D. C. (2009). BASL controls asymmetric cell division in *Arabidopsis*. *Cell* **137**, 1320-1330. doi:10.1016/j.cell.2009.04.018
- Drubin, D. G. and Nelson, W. J. (1996). Origins of cell polarity. *Cell* **84**, 335-344. doi:10.1016/S0092-8674(00)81278-7
- Engineer, C. B., Ghassemian, M., Anderson, J. C., Peck, S. C., Hu, H. and Schroeder, J. I. (2014). Carbonic anhydrases, EPF2 and a novel protease mediate CO₂ control of stomatal development. *Nature* **513**, 246-250. doi:10.1038/nature13452
- Francis, D., Davies, M. S. and Barlow, P. W. (2008). A strong nucleotypic effect on the cell cycle regardless of ploidy level. *Ann. Bot.* **101**, 747-757. doi:10.1093/aob/mcn038
- Genschik, P., Criqui, M. C., Parmentier, Y., Derevier, A. and Fleck, J. (1998). Cell cycle -dependent proteolysis in plants: identification of the destruction box pathway and metaphase arrest produced by the proteasome inhibitor mg132. *Plant Cell* **10**, 2063-2075. doi:10.2307/3870784
- Gong, Y., Alassimone, J., Varnau, R., Sharma, N., Cheung, L. S. and Bergmann, D. C. (2021a). Tuning self-renewal in the *Arabidopsis* stomatal lineage by hormone and nutrient regulation of asymmetric cell division. *eLife* **10**, e63335. doi:10.7554/eLife.63335
- Gong, Y., Varnau, R., Wallner, E.-S., Acharya, R., Bergmann, D. C. and Cheung, L. S. (2021b). Quantitative and dynamic cell polarity tracking in plant cells. *New Phytol.* **230**, 867-877. doi:10.1111/nph.17165
- Gonsalvez, D. G., Li-Yuen-Fong, M., Cane, K. N., Stamp, L. A., Young, H. M. and Anderson, C. R. (2015). Different neural crest populations exhibit diverse proliferative behaviors. *Dev. Neurobiol.* **75**, 287-301. doi:10.1002/dneu.22229
- Han, S.-K. and Torii, K. U. (2016). Lineage-specific stem cells, signals and asymmetries during stomatal development. *Development* **143**, 1259-1270. doi:10.1242/dev.127712
- Han, C., Liu, Y., Shi, W., Qiao, Y., Wang, L., Tian, Y., Fan, M., Deng, Z., Lau, O. S., De Jaeger, G. et al. (2020). KIN10 promotes stomatal development through stabilization of the SPEECHLESS transcription factor. *Nat. Commun.* **11**, 4214. doi:10.1038/s41467-020-18048-w
- Hara, K., Yokoo, T., Kajita, R., Onishi, T., Yahata, S., Peterson, K. M., Torii, K. U. and Kakimoto, T. (2009). Epidermal cell density is autoregulated via a secretory peptide, epidermal patterning factor 2 in *Arabidopsis* leaves. *Plant Cell Physiol.* **50**, 1019-1031. doi:10.1093/pcp/pcp068
- Homem, C. C. F. and Knoblich, J. A. (2012). *Drosophila* neuroblasts: a model for stem cell biology. *Development* **139**, 4297-4310. doi:10.1242/dev.080515

- Hunt, L. and Gray, J. E. (2009). The signaling peptide EPF2 controls asymmetric cell divisions during stomatal development. *Curr. Biol.* **19**, 864-869. doi:10.1016/j.cub.2009.03.069
- Jankele, R., Jelier, R. and Gönczy, P. (2021). Physically asymmetric division of the *C. elegans* zygote ensures invariably successful embryogenesis. *eLife* **10**, e61714. doi:10.7554/eLife.61714
- Jedrusik, A., Bruce, A. W., Tan, M. H., Leong, D. E., Skamagki, M., Yao, M. and Zernicka-Goetz, M. (2010). Maternally and zygotically provided Cdx2 have novel and critical roles for early development of the mouse embryo. *Dev. Biol.* **344**, 66-78. doi:10.1016/j.ydbio.2010.04.017
- Jones, A. R., Forero-Vargas, M., Withers, S. P., Smith, R. S., Traas, J., Dewitte, W. and Murray, J. A. H. (2017). Cell-size dependent progression of the cell cycle creates homeostasis and flexibility of plant cell size. *Nat. Commun.* **8**, 15060. doi:10.1038/ncomms15060
- Karimi, M., Bleys, A., Vanderhaeghen, R. and Hilson, P. (2007). Building blocks for plant gene assembly. *Plant Physiol.* **145**, 1183-1191. doi:10.1104/pp.107.110411
- Kubo, M., Udagawa, M., Nishikubo, N., Horiguchi, G., Yamaguchi, M., Ito, J., Mimura, T., Fukuda, H. and Demura, T. (2005). Transcription switches for protoxylem and metaxylem vessel formation. *Genes Dev.* **19**, 1855-1860. doi:10.1101/gad.1331305
- Lau, O. S., Song, Z., Zhou, Z., Davies, K. A., Chang, J., Yang, X., Wang, S., Lucyshyn, D., Tay, I. H. Z., Wigge, P. A. et al. (2018). Direct control of speechless by PIF4 in the high-temperature response of stomatal development. *Curr. Biol.* **28**, 1273-1280.e3. doi:10.1016/j.cub.2018.02.054
- Lauber, M. H., Waizenegger, I., Steinmann, T., Schwarz, H., Mayer, U., Hwang, I., Lukowitz, W. and Jürgens, G. (1997). The Arabidopsis KNOLLE protein is a cytokinesis-specific syntaxin. *J. Cell Biol.* **139**, 1485-1493. doi:10.1083/jcb.139.6.1485
- Lee, J. S., Hnilova, M., Maes, M., Lin, Y.-C., Putarjuna, A., Han, S.-K., Avila, J. and Torii, K. U. (2015). Competitive binding of antagonistic peptides fine-tunes stomatal patterning. *Nature* **522**, 439-443. doi:10.1038/nature14561
- Morin, X. and Bellaïche, Y. (2011). Mitotic spindle orientation in asymmetric and symmetric cell divisions during animal development. *Dev. Cell* **21**, 102-119. doi:10.1016/j.devcel.2011.06.012
- Muroyama, A. and Bergmann, D. (2019). Plant cell polarity: creating diversity from inside the box. *Annu. Rev. Cell Dev. Biol.* **35**, 309-336. doi:10.1146/annurev-cellbio-100818-125211
- Muroyama, A., Gong, Y. and Bergmann, D. C. (2020). Opposing, polarity-driven nuclear migrations underpin asymmetric divisions to pattern Arabidopsis stomata. *Curr. Biol.* **30**, 4549-4552. doi:10.1016/j.cub.2020.09.087
- Rowe, M. H., Dong, J., Weimer, A. K. and Bergmann, D. C. (2019). A plant-specific polarity module establishes cell fate asymmetry in the Arabidopsis stomatal lineage. *bioRxiv* doi:10.1101/614636
- Vatén, A., Soyars, C. L., Tarr, P. T., Nimchuk, Z. L. and Bergmann, D. C. (2018). Modulation of asymmetric division diversity through cytokinin and speechless regulatory interactions in the Arabidopsis stomatal lineage. *Dev. Cell* **47**, 53-66.e5. doi:10.1016/j.devcel.2018.08.007
- Wang, S., Zhou, Z., Rahiman, R., Lee, G. S. Y., Yeo, Y. K., Yang, X. and Lau, O. S. (2021). Light regulates stomatal development by modulating paracrine signaling from inner tissues. *Nat. Commun.* **12**, 3403. doi:10.1038/s41467-021-23728-2
- Zhang, Y., Wang, P., Shao, W., Zhu, J.-K. and Dong, J. (2015). The BASL polarity protein controls a MAPK signaling feedback loop in asymmetric cell division. *Dev. Cell* **33**, 136-149. doi:10.1016/j.devcel.2015.02.022
- Zhang, Y., Guo, X. and Dong, J. (2016). Phosphorylation of the polarity protein BASL differentiates asymmetric cell fate through MAPKs and SPCH. *Curr. Biol.* **26**, 2957-2965. doi:10.1016/j.cub.2016.08.066